Available online at www.sciencedirect.com
SCIENCE DIRECT
Polymer 46 (2005) 6429–6436
polymer
www.elsevier.com/locate/polymer

Strain amplitude response and the microstructure of PA/clay nanocomposites

T. Wan[a], M.J. Clifford[a,*], F. Gao[b], A.S. Bailey[c], D.H. Gregory[c], R. Somsunan[c]

[a]School of Mechanical, Materials and Manufacturing Engineering, The University of Nottingham, University Park, Nottingham NG7 2RD, UK
[b]School of Biomedical and Natural Science, Nottingham Trent University, Clifton Lane, Nottingham NG11 8NS, UK
[c]School of Chemistry, The University of Nottingham, University Park, Nottingham NG7 2RD, UK

Received 10 November 2004; received in revised form 16 March 2005; accepted 1 April 2005
Available online 21 June 2005

Abstract

Polyamide 6/clay nanocomposites (PAn, where n is the mass fraction of clay) with various clay loading were prepared by melt compounding in a twin screw extruder. Exfoliation of clay in a PA matrix was confirmed by X-ray diffraction. Strain amplitude response of PAn in both melt and solution states has been investigated. In the melt state, critical strain amplitude of PAn is sensitive to strain amplitude response and decrease logarithmically with increasing clay loading. The elastic moduli (G') of PAn are reversible under frequency loop sweeps. Comparisons of strain amplitude response in both melt and solution states have been conducted. Two different responses have been observed: strain thinning in the melt state and weak strain overshoot in the solution state. FTIR studies show that amide II band of PAn shifts toward high wavenumbers, but amide I band and N–H stretching vibration are independent of clay loading. We suggest that two types of strain amplitude response of PAn can be explained: strain thinning which is dominant in PAn caused by physical adsorption and entanglement of PA chains on nanoclays and weak strain overshoot caused by weak bonds between PA chains and nanoclays.

Keywords: Polyamide 6; Nanocomposites; Microstructure

1. Introduction

Polymer–clay nanocomposites have attracted considerable scientific and industrial interests because they exhibit significant improvements in physical and mechanical properties over virgin polymers with minimal increase in density [1].

Recently, great interest has focused on the rheological properties of polymer/clay nanocomposites [2–5]. In general, two reasons drive the studies of the rheology of nanocomposites. From an engineering perspective, determining the rheological properties of nanocomposites is vital to optimize processing during manufacture of engineering components. It guides and improves melt processability to assist flow in molded parts and to impregnate continuous glass fibres to form composites with nanocomposite matrices [6]. From a scientific research point of view, nanocomposites provide an ideal nanoscale space to study confined polymers and examine the effect of nanoclays on the rheology of nanocomposites [7]. Furthermore, a thorough understanding of the rheological properties of nanocomposites is essential to tailor nanocomposites and govern the ultimate mechanical performance for various applications.

Previous studies on the rheology of nanocomposites have shown that nanocomposites are sensitive to small deformation. They exhibit pseudo solid-like behavior and yield stress to a small oscillatory shear [8,9]. Higher viscosities and shear thinning properties can be observed for nanocomposites at relatively low shear rate at which the matrix exhibits a Newtonian flow, but when the shear rate increases, the viscosities of nanocomposites decrease significantly [10]. The results can be attributed to the presence of anisotropic nanoclays forming a network structure, which can be broken down under a large shear deformation. Since nanoclays significantly affect the rheological properties of nanocomposites, the network formation would be related to the microstructure of

* Corresponding author. Tel.: +44 115 8466134; fax: +44 115 9513800.
E-mail address: mike.clifford@nottingham.ac.uk (M.J. Clifford).

0032-3861/$ - see front matter © 2005 Elsevier Ltd. All rights reserved.
doi:10.1016/j.polymer.2005.04.105

nanocomposites and interaction between nanoclays and polymer matrix. However, interaction and the mechanism for the formation of the microstructure are not readily understood.

Strain amplitude response of complex melts could detect complex interaction and reflect changes in the microstructure of the melts. In general, the elastic moduli (G') and the viscous moduli (G'') are chosen for characterizing changes to the microstructure, so four types of strain amplitude response to the microstructure changes can be classified [11]: type I, strain thinning (G', G'' both decrease); type II, strain hardening (G', G'' both increase); type III, weak strain overshoot (G' decrease, G'' increase followed by decrease); type IV, strong strain overshoot (G', G'' both increase followed by decrease).

In order to explore the microstructure of nanocomposites, an experimental investigation is conducted to determine strain amplitude response of polyamide 6/clay nanocomposites (PAn, where n is the mass fraction of clay) in both melt and solution states. PAn are studied because a high content of exfoliation takes place during the melt compounding process compared to other polymers [12,13]. In the exfoliated system, single clay layers interact with PA chains, providing a way to explore interaction between nanoclays and PA chains at the molecular level via rheology measurements. Strain amplitude is a powerful method to probe the changes of the microstructure, especially when highly anisotropic layers are dispersed in a polymer matrix. In this paper, a special emphasis is placed on strain amplitude response in both melt and solution states. FTIR has also been used to evaluate interaction between PA chains and nanoclays.

2. Experimental method

2.1. Materials

Ultramid B3 polyamide 6 (PA) was supplied by BASF in the form of granules. Organo-clay (NTU-1) modified by organophilic surfactants was provided by Nottingham Trent University. All materials were dried at 80 °C under vacuum before testing.

2.2. Preparation of PAn and their solutions

PA and clay were melt blended at 240 °C in a 16 mm twin screw extruder at feeding rate of 15%, $L/D=$ 24,400 rpm. The extruded strands were palletised and dried under vacuum at 80 °C for 10 h before testing. Polyamide 6 denotes PA and Polyamide 6/clay nanocomposites denote PAn, where $n=1$, 3, 5, 8, 10 is the mass fraction of clay.

Nanocomposite solutions can be prepared by directly mixing PAn and 99% formic acid. Firstly, 20 g of PAn were dissolved in 80 g of formic acid at 40 °C for 3 h. The solutions become light yellow after PAn had fully dissolved. In order to compare experiment results, PAc (the mixture of PA and organo-clay) and PA solutions were prepared as two references. A mixture of 18 g of PA and 2 g of organo-clay (NTU-1) powder were added to 80 g of formic acid and mixed well to form PAc solution. 20 g of PA dissolved in 80 g of formic acid to form PA solution.

2.3. Wide angle X-ray diffraction (WAXD)

Wide angle X-ray diffraction was used to measure the dispersion of clay in PA matrix. All data were collected using a Philips Xpert θ–2θ powder diffractometer in Bragg-Brentano, flat plate geometry with Cu Kα radiation. Samples were prepared for the diffraction experiment by cutting to the size of the plate aperture. The samples were then affixed to the plate with adhesive before performing the experiment. Data were collected for PA, the organo-clay (NTU-1) and all PAn samples as step scans from $1.5° \leq 2\theta \leq = 30°$ with a step of 0.02° and a time/step of 1.25 s. Peak positions and phase purity were evaluated using Philips APD and IDENTIFY routines respectively. Fig. 1 shows WAXD patterns of NTU-1, PA and PAn. The d_{001} spacing for the clay was calculated automatically from Bragg's law, $n\lambda = 2d \sin\theta$.

2.4. Rheology characterization

Rheology tests were performed on a Bohlin CVOR200 Rheometer. A pair of 25 mm diameter parallel plates with a 1 mm gap size was used in all tests. Strain amplitude sweeps were conducted from 0.1 to 100% at three different angular frequencies ($\omega=0.5$, 1 and 10 rad/s). The elastic moduli (G') and the viscous moduli (G'') as the function of strain amplitude (γ) were recorded. For recovery measurements, frequency loop sweeps were carried out ranged from 0.1 to 100 rad/s at a fixed strain amplitude ($\gamma=0.5\%$) to ensure

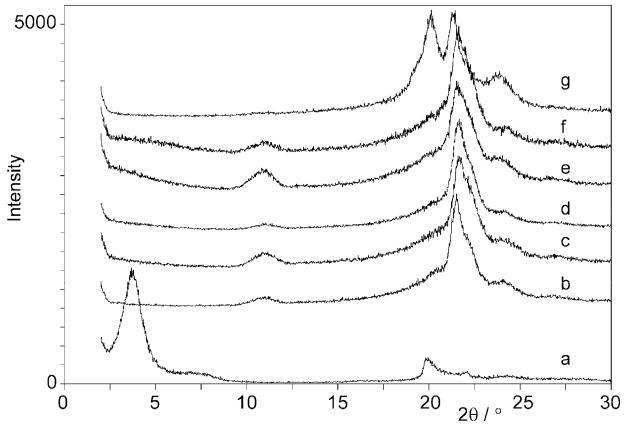

Fig. 1. Powder X-ray diffraction profiles for organo-clay (NTU-1) (a) and PAn nanocomposites, PAn, with mass fractions of clay, $n=1$, 3, 5, 8, 10 shown from (b)–(f), respectively. The diffraction pattern for PA is shown for comparison (g).

that the measurements were taken within the linear viscoelastic range.

Sample disks for PAn with 1 mm thickness were prepared by compression moulding at 240 °C for 3 min. After loading between a pair of parallel plates with 1 mm gap, the sample disks were annealed for 5 min to ensure that they were fully melted and in an equilibrium state (240 °C). All measurements were conducted under a nitrogen atmosphere to avoid oxidative degradation.

Sample disks for PAn solutions were prepared by squeezing 3 ml of solutions between a pair of parallel plates with 1 mm gap and annealed for 5 min. The measurements were carried out at 25 °C under a nitrogen atmosphere.

2.5. Fourier transform infrared spectroscopy (FTIR)

Samples for FTIR analyses were prepared as follows: 0.3 g of PA and PAn granules were dissolved in 10 g formic acid, respectively. 20 μl of the solution was coated on a KBr plate and then evaporated in a vacuum oven at 70 °C for 10 h to ensure thin films were produced. FTIR analysis was preformed on a Bruker Tensor 27 FTIR spectrometer. FTIR spectra were recorded from 4000 to 400 cm^{-1} at a resolution of 4 cm^{-1}.

3. Results and discussion

3.1. Characterization of exfoliation of PAn nanocomposites

Fig. 1 shows the WAXD patterns of the organo-clay (NTU-1), PA and PAn. The organo-clay (curve a) has a sharp peak at $2\theta = 3.6°$ corresponding to a [001] interlayer distance $d_{001} = 2.45$ nm. Compared to the organo-clay, nanocomposites (curves b–f) with various clay loading from 1–10 wt% do not exhibit an equivalent peak in the range of 2–10°. The absence of the [001] peak demonstrates that the organo-clay is well dispersed within the PA matrix. Furthermore, in order to confirm the formation of nanocomposites, the crystalline patterns of PA and PAn nanocomposites were studied in the range 10–30°. Previous studies have demonstrated that nanodispersed clay could affect the crystalline phase of the PA matrix, inducing a phase transition from the α to γ crystalline phase. The α crystalline phase has twin peaks at 20.3° (α1) and 23.7° (α2) while the peaks of the γ crystalline phase are located at 2θ = 11 and 21.8° [14,15]. Fig. 1 (curve g) shows that the sample of PA exists with both the α and γ phases present with corresponding peaks at 20.3° (α1), 21.8° (γ) and 24° (α2), respectively. However, PAn exhibits two signature peaks that can be ascribed to the γ phase at 11 and 21.8° and conversely no evidence of the peak at 20.3 suggestive of the α phase, as shown in Fig. 1 (curves b–f). The crystalline phase transition of PAn from α to γ is an additional strong indication of clay exfoliation and formation of nanoclays in the PA matrix.

3.2. Strain amplitude response of PAn in the melt state

To characterize the microstructure of PAn, the transition from linear to nonlinear viscoelastic behaviour under strain amplitude has been studied. Strain amplitude dependence of the elastic moduli (G') for PA and PAn were measured from 0.1 to 100% at the three frequencies ($\omega = 0.5$, 1, 10 rad/s). The elastic moduli (G') of PA and PA10 are presented here as typical results. The elastic moduli (G') of PA and PA10 at the three frequencies ($\omega = 0.5$, 1, 10 rad/s) are superposed with application of a normalized shift in Fig. 2.

Fig. 2 shows that the elastic moduli (G') of PA and PA10 at different frequencies can be superposed and the transition of linear to nonlinear viscoelastic behavior for PA10 is only a function of strain amplitude and is independent of frequency. All other nanocomposites measured also show the similar independent transition, so the critical transition of the elastic moduli (G') is denoted critical strain amplitude (γ_c). For purposes of comparison of critical strain amplitude (γ_c), the elastic moduli (G') and the viscous moduli (G'') of PAn are measured at a fixed frequency and temperature ($\omega = 1$ rad/s and 240 °C). The elastic moduli (G') of PAn are normalized by the values in the linear region at low strain amplitude and plotted against strain amplitude in Fig. 3.

The normalized elastic moduli (G') exhibit a linear region at low strain amplitude and nonlinear region at high strain amplitude. The region of linear viscoelastic behaviour for PA extends to a strain of 18%, but the presence of nanoclays is very sensitive to small strains and causes a sharp decrease in the normalized elastic moduli (G') for PAn beyond critical strain amplitude (γ_c). More clay loading results in lower critical strain amplitude (γ_c) and

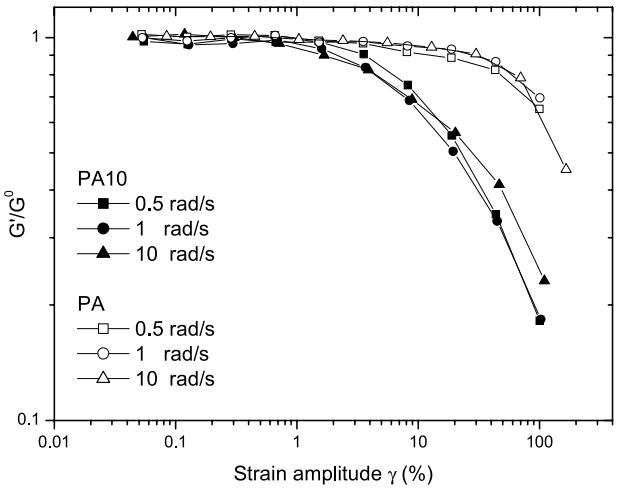

Fig. 2. Strain amplitude dependence of the normalized elastic moduli (G'/G_0) of PA and PA10 at different angular frequencies ($\omega = 0.5$, 1, 10 rad/s) (the open and closed symbols are for the PA and PA10, respectively).

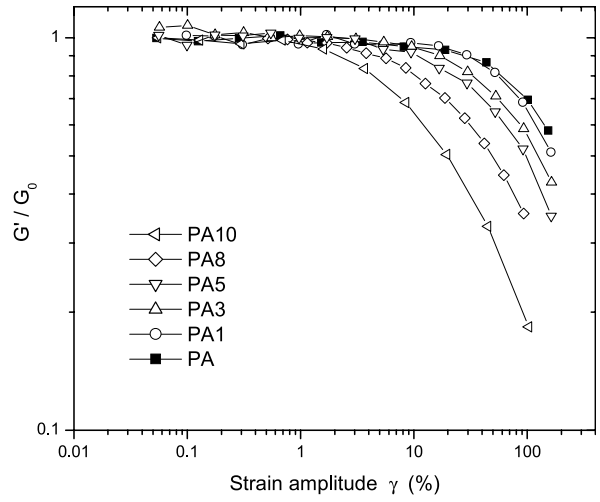

Fig. 3. Strain amplitude dependence of the normalized elastic moduli (G'/G_0) at a constant angular frequency ($\omega=1$ rad/s) (the open and closed symbols are for the PA and PAn, respectively).

smaller linear viscoelastic range. Critical strain amplitude (γ_c) is shown in Fig. 4 as a function of clay loading.

Interestingly, critical strain amplitude (γ_c) of PAn decreases logarithmically with clay loading. Critical strain amplitude (γ_c) dependence of clay loading can be explained by the formation of a network. Previous studies suggested that the anisotropic nanoclays could be aligned to the flow direction under strain amplitude and rupture clay particle–particle interaction [10]. It is expected that the network structure in nanocomposites should gradually form with increasing clay loading and probably be related to the presence of either highly anisotropic nanoclays or adsorption of PA chains on the surface of nanoclays. The formation of a network is also related to the types of organo-clay. Various organo-clays can affect the rheological properties of eventual nanocomposites [16]. In order to explore the details of network formation and the microstructure for PAn, the angular frequency loop sweeps ($\omega=$

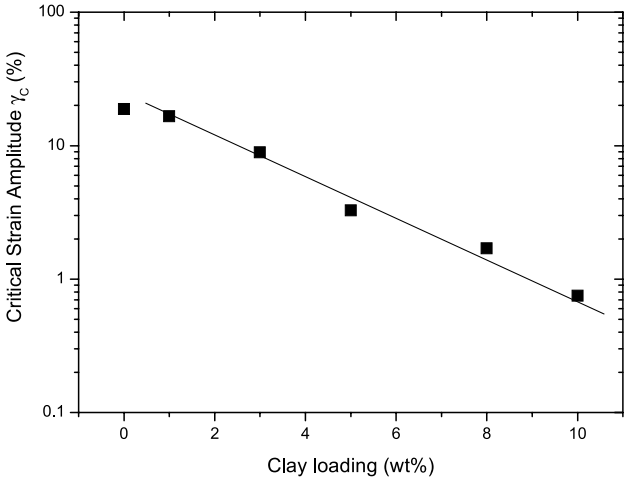

Fig. 4. Critical strain amplitude (γ_c) as a function of clay loading.

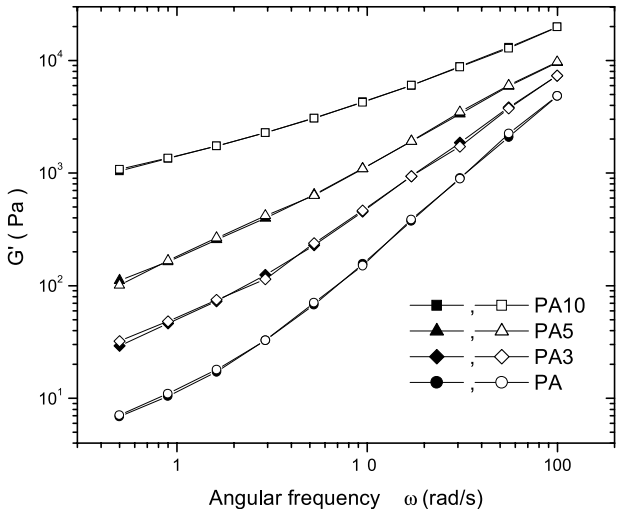

Fig. 5. Elastic moduli (G') of PA and PAn as a function of angular frequency loop ($\omega=0.5$–100 rad/s). The closed and opened symbols represent increasing and decreasing angular frequency sweeps respectively.

0.5–100 rad/s) are performed at 0.5% strain amplitude to make sure that PAn has been measured in the linear region. The elastic moduli (G') of PAn shown in Fig. 5, shows that the process is recoverable.

The elastic moduli (G') of PAn are exactly the same in both increasing the angular frequencies and the reverse process. These results suggest that the network can rebuild quickly with the removal of the applied angular frequencies. As shown in Fig. 2, critical strain amplitude (γ_c) is independent of frequencies under strain amplitude. This demonstrates that the breakdown of the network is independent of the mechanical response of the PA matrix and is a function of clay loading. The breakdown and recovery of the network due to strain amplitude in PAn may be related to physical adsorption between nanoclays and PA chains. Obviously physical adsorption is not as strong as crosslinked systems, since the network can be quickly recovered. Physical adsorption occurs on the interface of nanoclays because of the presence of an interfacial surface energy. According to the thermodynamic equation: $\Delta\sigma = \Delta U - \Delta(TS) = \nu_1 s + \mu n$. Physical adsorption depends on the values of the specific surface energy (ν_1) and surface area (s). The number of moles of adsorbed polymers (n) increases with the value of $\nu_1 s$. μ is the chemical potential of the adsorbed polymers. In general, the specific surface energy (ν_1) of clay is very large. For example, the specific surface energy of mica is about 4500 mN/m in vacuum [17]. When clay is exfoliated into a PA matrix, the large specific surface area of nanoclays creates an attractive force between the surface of nanoclays and the PA chains because of the large value of ν_1s. It is to be expected that the amount of absorbed PA chains increase with increasing clay loading. The result of this adsorption is characterized as physical (or Van der Waals) adsorption. Physical adsorption of a polymer on a solid surface can be described by the

Loop-train-tail model [18]. The entanglements of PA chains significantly increase on the surface of nanoclays due to physical adsorption. We expect that the sum of the surface areas of nanoclays increase with clay loading, so the amount of entanglement caused by this adsorption increases with clay loading. Interaction caused by physical adsorption can be monitored by strain amplitude response.

Figs. 3 and 6 show that the elastic moduli (G') and the viscous moduli (G'') of PAn both decrease with increasing strain amplitude. This type of strain amplitude response of PAn in the melt state belongs to type I, strain thinning. For small strain amplitude, the rates of entanglement and disentanglement of PA chains on nanoclays are equal, so the elastic moduli (G') and the viscous moduli (G'') are constant in this equilibrium state. When strain amplitude increases, PA chains untangle from nanoclays and align in the flow direction, so the network is easily lost. Strain thinning effects become significant with increasing clay loading. At high clay loading, the large amount of entanglements is sensitive to small strain amplitude. The increasing entanglements near the surface of nanoclays cause the local drag to increase and critical strain amplitude (γ_c) to decrease. Therefore, the threshold of strain thinning becomes more sensitive to smaller strain amplitude.

Earlier works [19] on end-tethered polymer/clay nanocomposites showed that poly(caprolactone) nanocomposites at large strain amplitude (150%) for 3 h, align in the flow direction. Because the clay particles are dispersed in the polymer matrix as individual layers and stacks of layers are anisotropic particles with high aspect ratio and quite large surface areas, the breakdown of the microstructure may be due to orientation of clay particles in the flow direction when a shear force is applied. Hydrotalcite-like/clay exhibits thixotropic behavior and the viscosities depend on the previous shear history [20,21]. However, it is unlikely to observe thixotropic behavior and alignment of nanoclays in PAn during these tests, probably because strain amplitude is only imposed for a relatively short time in which the obvious alignment of nanoclays can not be created.

Thus, the most reasonable explanation of strain amplitude response of PAn in the melt state is that the large nanoclay surface easily absorbs PA chains and forms a physical network. It also worth noting that the end-tethered PCL nanocomposites exhibit shear thickening which is caused by the strong interaction between nanoclays and PCL chains [19]. It is expected that the special interaction exists between nanoclays and PA chains, even if it is not as strong as end-tethered nanocomposites. Only strain thinning of PAn could be observed in the melt state, because physical adsorption of PA chains on nanoclays which caused the entangled points to disengage easily from nanoclays is dominant in PAn. Thus, the special interaction between nanoclays and PA chains cannot be easily observed in the melt state.

3.3. Strain amplitude response of PAn in the solution state

In order to explore the special interaction under strain amplitude, the entanglements of PA chains near nanoclay surface must be weakening. The simple way to reduce strain thinning response is to dissolve PAn in a solvent. In our tests, formic acid is used to dissolve PAn. By this method, clay loading in PAn solutions can be greatly diluted. For example, PA5 solution only has 1% clay loading. It not only reduces the interaction due to physical adsorption and the aggregation between nanoclays, but also substantially decreases the entanglements of PA chains near nanoclays. However, we expect that the special interaction between nanoclays and PA chains becomes predominant in PAn solutions.

The elastic moduli (G') and the viscous moduli (G'') of PAn in both melt and solution states respectively as a

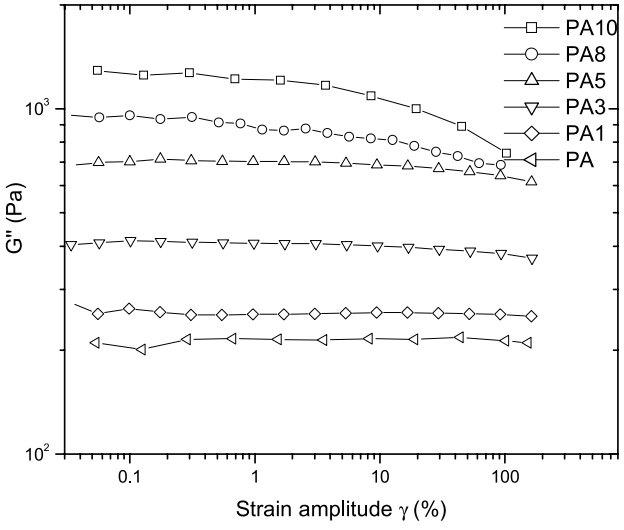

Fig. 6. Viscous moduli (G'') of PA, PAn and PAc in the melt state as a function of strain amplitude at a constant angular frequency ($\omega = 1$ rad/s).

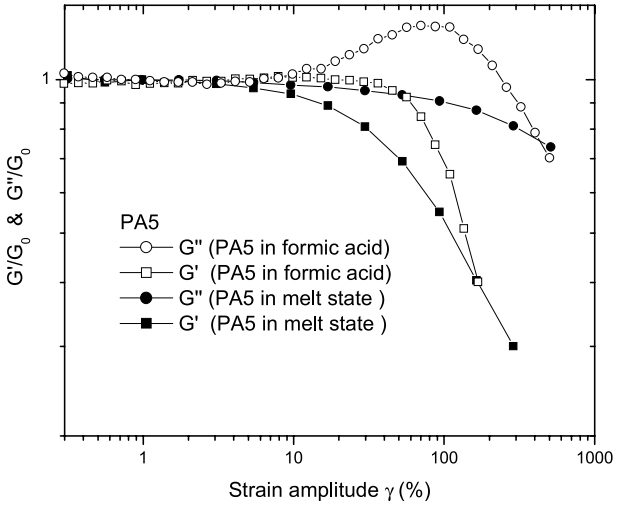

Fig. 7. Reduced moduli G'/G_0 and G''/G_0 of PA5 in both the melt and the solution states as a function of strain amplitude at a constant angular frequency ($\omega = 1$ rad/s) PA5 solution shows weak strain overshoot.

function of strain amplitude have been tested. The results for PA5 are presented here. Fig. 7 shows that strain amplitude response of PA5 in both melt and solution states. The elastic moduli (G') and the viscous moduli (G'') both decrease with increasing strain amplitude for PA5 in the melt state, which corresponds to strain thinning. However, the viscous moduli (G'') of PA5 solution first increases followed by a decrease with increasing strain amplitude while the elastic moduli (G') decreases. Obviously the type of strain amplitude response of PA5 solution belongs to type II, weak strain overshoot. Weak strain overshoot is not as common as strain thinning. It can be observed in some complex fluids, such as xantham gum solution [16], fumed silica suspensions [22] and some electrorheological (ER) fluids under an electric field [23], but little has been understood about its mechanism, because the viscous moduli (G'') in the nonlinear region are more difficult to analyse. Xantham gum shows this response because it has long side chains, which can form a weak complex structure. Fumed silica suspension shows this response because it has a weak filler network. The results show that this strain response is complicated and related to the diverse interactions in the system. This response can be described by a network model which consider that the distribution of network junction is determined by creation and loss rate of junctions [24]. For strain thinning, the creation rate is negative, while the loss rate is positive, so the elastic moduli (G') and the viscous moduli (G'') decrease with increasing strain amplitude beyond critical strain amplitude. For weak strain overshoot, the creation and loss rates are positive and the loss rate is larger than the creation rate. When a strain is imposed beyond critical strain amplitude, the complex structure resists the deformation until the viscous moduli (G'') reaches a maximum value. If the strain continues to increase, the complex structure is destroyed by a large strain, and the viscous moduli (G'') decreases. The viscous moduli (G'') increases followed by a decrease while the elastic moduli (G') decreases, because the destruction rate is faster than the creation rate. In order to confirm weak strain overshoot caused by the interaction between nanoclays and PA chains, the viscous moduli (G'') of PA, PAn and PAc solutions are shown in Fig. 8.

It is apparent that the viscous moduli (G'') of PAn solutions increase and then decrease with strain amplitude. The intensity of weak strain overshoot becomes stronger with increasing clay loading. PA1 solution only shows very small weak strain overshoot, but PA3, PA5, PA8 and PA10 show obvious weak strain overshoot and the interaction becomes significant. Fig. 8 also shows that strain amplitude transition of the viscous moduli (G'') from linear to nonlinear becomes smaller with increasing clay loading. This demonstrates that interaction is dependant on clay loading and becomes stronger with increasing nanoclay content. PA and PAc solutions as references have been studied and are shown in Fig. 8. In contrast with PAn solution, PA and PAc solutions exhibit Newtonian behavior

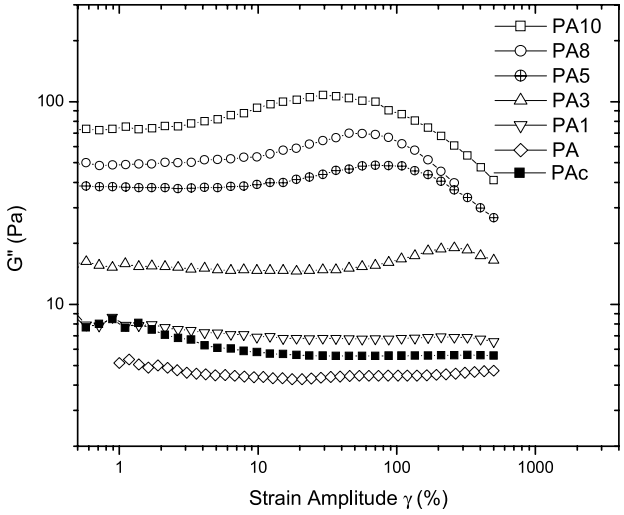

Fig. 8. Viscous moduli (G'') of PA, PAn and PAc in the solution state as a function of strain amplitude at a constant angular frequency ($\omega = 1$ rad/s).

instead of weak strain overshoot. Fig. 9 shows the phase angles of PA, PAc and PA5 as a function of strain amplitude. Compared to PA5 solution, the phase angles of PA and PAc solutions are nearly 90° and independent of strain amplitude. Formic acid in PAn solution is not the cause for weak strain overshoot. Thus, it is expected that weak strain overshoot is caused by the interaction between PA chains and nanoclays.

3.4. FTIR analysis

In order to examine the interaction between PA chains and nanoclays which resulted in weak strain overshoot, FTIR was used to monitor amide group vibrations of PA chains and characterize the microstructure of PAn. The major spectral bands of PA in the range of 3600–2800 and 1750–1550 cm^{-1} are summarized in Table 1 [25,26].

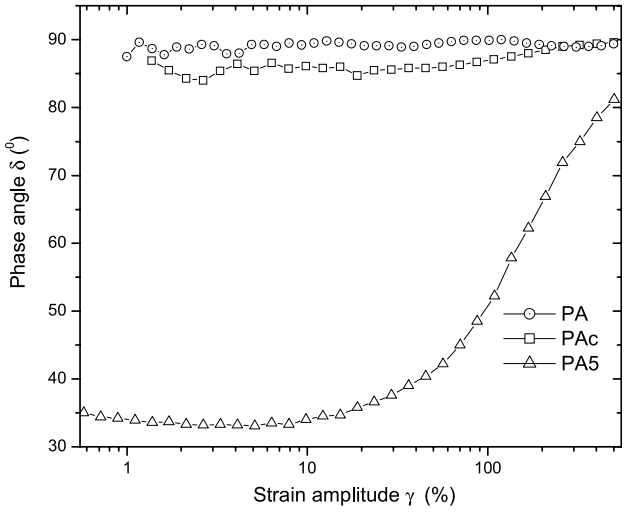

Fig. 9. Phase angle of PA,PA5 and PAc in the solution state as a function of strain amplitude, where PA and PAc show Newtonian behavior.

Table 1
Major spectral bands of PA in the range of 3600–2800 and 1750–550 cm^{-1}

Absorbance bands (cm^{-1})	Major contribution to vibrations
3300	Hydrogen-bonded N–H stretching vibration
3070	Overtone of amide II band and Fermi resonance of N–H vibration
2930	Asymmetric CH_2 stretching vibration
2860	Symmetric CH_2 stretching vibration
1640	C=O stretching vibration (amide I band)
1540	N–H deformation vibration (amide II band)

Fig. 10 shows that FTIR spectra of PA, PAn and PAc at room temperature are in the range of 3600–2800 cm^{-1}. The strong band attributed to hydrogen bonded N–H stretching vibration with C=O can be observed at 3300 cm^{-1}. The two bands at 2930 and 2858 cm^{-1} are attributed to CH_2 stretching. The spectra of PAn are very similar to that of PA, except for the different spectral bands at the 3086 and 3100 cm^{-1}. Table 1 shows that the spectral band of PA at 3086 cm^{-1} belongs to Fermi-resonance of N–H vibration and the overtone of amide II. The spectral shift from 3086 to 3100 cm^{-1} can be observed in PAn, but no shift appears in PAc. Fig. 11 shows that the FTIR spectra of PA, PAn, PAc and organo-clay (NTU-1). The strong spectral band of PA at 1642 cm^{-1} is attributed to C=O stretching vibration of the amide I band. Another spectral band at 1548 cm^{-1} of PA is attributed to N–H vibration of the amide II band. The spectra of PA and PAc are very similar at 1548 cm^{-1}, but remarkable shifts from 1548 to 1568 cm^{-1} can be observed for PAn. According to Figs. 10 and 11, the overtone amide II band of PAn shifting from 3086 to 3100 cm^{-1} with low intensities can be observed at approximately twice of the shift of the amide II band shifting from 1548 to 1568 cm^{-1}. No spectral band at 1586 cm^{-1} appears for organo-clay (NTU-1). We expect that the amide group is very active and easy interacts with nanoclays. The amide II vibration of PAn shift to higher wavenumbers and the intensity increases with clay loading. However, the positions of amide I vibration and N–H stretching vibration are independent of clay loading. In general, hydrogen bonding has the effect of moving the N–H deformation bands to high frequencies. This shift depends on the strength of the hydrogen bonds [26]. The differences in amide II band for PAn and PA demonstrate that the special interaction (maybe hydrogen bonds) between N–H group and nanoclays exists. Recently, studies have shown that the deformation behavior of nanoclays in PA/clay nanocomposites have been evaluated by FTIR. Results show that Si–O stretching vibration of nanoclays could be shifted to lower wavenumbers by stress deformation and shifted back to its original position when the stress is released [27,28].

The fact that weak strain overshoot can be found in the solution and not in the melt state can be explained by a bimodel response as shown in Fig. 12. Most of PA chains are entangled on the surface of nanoclays by physical adsorption. In the melt state, this effect is dominant and results in strain thinning. On the other hand, some of PA chains weakly bond to nanoclays, so weak strain overshoot becomes predominant and can be observed in the solution state.

4. Conclusions

Strain amplitude response of PA and PAn have been studied in both melt and solution states. Critical strain amplitude (γ_c) logarithmically decreases with increasing clay loading because of the formation of a network. The elastic moduli (G') of PAn are completely reversible under angular frequency loop sweeps. Strain thinning of Pan in the melt state and weak strain overshoot in the solution state can be observed with increasing strain amplitude. FTIR studies show that amide II band of PAn shifts toward high

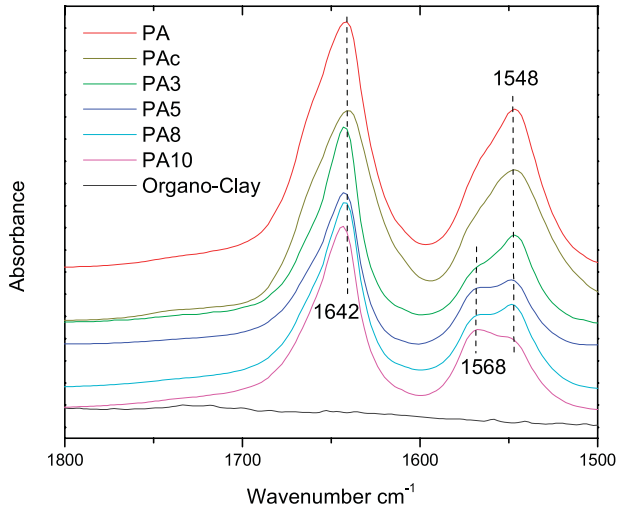

Fig. 10. FTIR spectra of PA, PAn, organo-clay (NTU-1) and PAc in the range of 1800–1500 cm^{-1}.

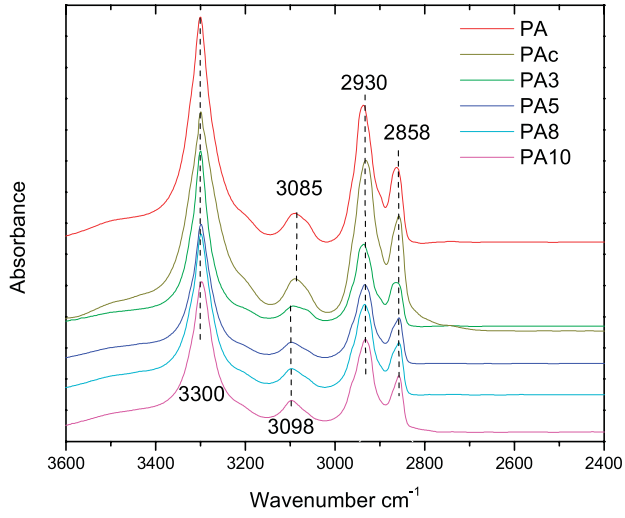

Fig. 11. FTIR spectra of PA, PAn and PAc in the range of 3600–2400 cm^{-1}.

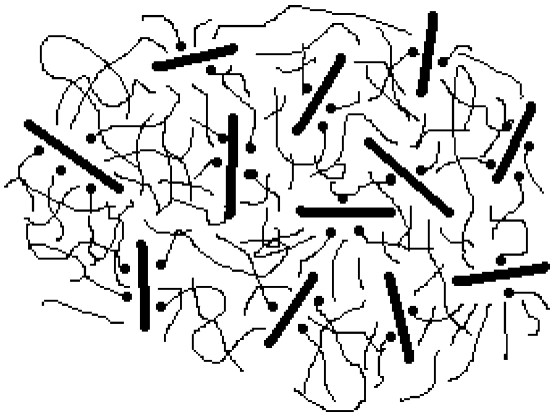

Fig. 12. Schematic illustration of the microstructure of PAn. Most PA chains are absorbed by nanoclays due to physical adsorption. Some of PA chains are weakly bonded to nanoclays (black dots).

wavenumbers, and the intensity increases with clay loading. Two types of interaction exist in PAn nanocomposites: strain thinning which is dominant in nanocomposites caused by adsorption of PA chains on nanoclay and weak strain overshoot caused by weak bonds between PA chains and nanoclays.

References

[1] Pinnavaia TJ, Beall GW. Polymer–clay nanocomposites. New York: Wiley; 2000 [chapter 6].
[2] Krishnamoorti R, Vaia RA, Giannelis EP. Chem Mater 1996;8: 1728–34.
[3] Ren J, Silva AS, Krishnamoorti R. Macromolecules 2000;33: 3739–46.
[4] Galgali G, Ramesh C, Lele A. Macromolecules 2001;34:852–8.
[5] Ren J, Krishnamoorti R. Macromolecules 2003;36:4443–51.
[6] Daniel PNV, Harald ENB, Stephen JP. SAMPE Eur Conf Exhibition 2004;181–6.
[7] Giannelis EP, Krishnamoorti R, Manias E. Advances in polymer science. Berlin: Springer; 1999 p. 108–47.
[8] Krishnamoorti R, Giannelis EP. Macromolecules 1997;30:4097–102.
[9] Zhong Y, Wang S-Q. J Rheol 2003;47(2):483–95.
[10] Krishnamoorti R, Ren J, Silva AS. J Chem Phys 2001;114(11): 4968–78.
[11] Hyum K, Kim SH, Ahn KH, Lee SJ. J Non-Newtonian Fluid Mech 2002;107:51–65.
[12] Cho JW, Paul DR. Polymer 2001;42:1083–94.
[13] Shah RK, Paul DR. Polymer 2004;45:2991–3000.
[14] Liu X, Wu Q. Polymer 2002;43:1933–6.
[15] Kyotani M. J Polym Sci 1979;17:103–14.
[16] lee KM, Han CD. Polymer 2003;44:4573–88.
[17] Utracki LA. Clay-containing polymeric nanocomposites. Shawbury: Rapra Technology Ltd; 2004 [Part 3].
[18] Richard AL, Jones, Richards RW. Polymers at surface and interfaces. Cambridge, UK: Cambridge University Press; 1999.
[19] Krishnamoorti R, Giannelis EP. Langmuir 2001;17:1448–52.
[20] Li S-p, Huo W-g, Sun D-j, Guo P-z, Jia C-x. Langmuir 2003;19: 3172–7.
[21] Larson RG. The structure and rheology of complex fluids. UK: Oxford University Press; 1999 [chapter 6].
[22] Yziquel F, Carreau PJ, Tanguy PA. Rheol Acta 1999;38:14–25.
[23] Parthasarathy M, Klingenberg DJ. J Non-Newtonian Fluid Mech 1999;81:83–104.
[24] Sim HG, Ahm KH, Lee SJ. J Non-Newtonian Fluid Mech 2003;112: 237–50.
[25] Wu Q, Liu XH, Berglund LA. Polymer 2002;43:2445–9.
[26] Socrates G. Infrared and Raman characteristic group frequencies. 10. New York: Wiley; 2001 [chapters 9, 10 and 21].
[27] Loo LS, Karen K, Gleason K. Polymer 2004;45:5933–9.
[28] Loo LS, Gleason KK. Macromolecules 2003;36:2587–90.